Phase control of a two-photon transition with shaped femtosecond laser-pulse sequences

A. Präkelt, M. Wollenhaupt, C. Sarpe-Tudoran, and T. Baumert*
University of Kassel, Institute of Physics and Center for Interdisciplinary Nanostructure Science and Technology (CINSaT), Heinrich-Plett-Strasse 40, D-34132 Kassel, Germany
(Received 11 August 2004; published 13 December 2004)

Phase effects in a quantum control experiment on the two-photon transition $4s \leftarrow\leftarrow 3s$ of atomic sodium are studied. In our experiment, we combine the generation of phase-locked interferometrically generated pulses with pulse-shaping techniques to study in detail the interplay of optical and quantum-mechanical phases. Subtle differences in the physical realization of the pulse sequences produce large difference in the control objective—the 4*s* population. The control mechanisms of more complex pulse sequences generated by periodic and discontinuous phase-modulation functions are investigated systematically and analyzed on the basis of quantum-mechanical interference.

DOI: 10.1103/PhysRevA.70.063407 PACS number(s): 32.80.Qk, 42.65.Re, 32.80.Wr

The availability of ultrashort laser pulses and the ability to manipulate them have sped up the field of observation and control of atomic and molecular dynamics, with prospects for applications in physics, biology, chemistry, and engineering [1–4].

As one observation and control instrument, interferometrically generated pairs of femtosecond pulse sequences have been established. Pulse sequences which are, for instance, used in multidimensional spectroscopy approaches are especially suitable to study temporal phase effects in quantum-mechanical systems since the first pulse excites the system and defines the initial temporal phase while the second pulse (and eventually further pulses) interacts with the system, delivering relative temporal phases with interferometric accuracy [5–12]. In addition, pulse-shaping techniques [13–15] further expanded the range of applications of femtosecond laser pulses as an efficient tool for quantum control [16–23].

Here, we combine both techniques—the interferometric generation of femtosecond laser pulses and pulse-shaping technology—to study the role of the optical and quantum-mechanical phases on a two-photon transition on sodium atoms. The insights obtained from pure phase-control experiments using phase-locked pulse sequences are transferred to the analysis of our pulse-shaping results. This approach permits us to decompose a complex excitation scheme into more elementary steps that highlight the underlying physical mechanisms. The use of femtosecond laser pulses to control a nonresonant two-photon transition has been reported for interferometrically delayed pulses [6] and pulse shaping [24,25]. Moreover, adaptive closed-loop optimization of a two-photon transition has been investigated [26]. The control of a resonant two-photon transition has been studied in [27]. In addition to phase shaping, polarization shaping [28] has been implemented to control an atomic two-photon transition [29] and the multiphoton ionization of molecules [30]. Recently, pulse-shaping techniques were used to control multiphoton transitions of dyes in microscopy [31]. In our contribution, we analyze the quantum control of a two-photon transition with two pulses, one of which is phase modulated in addition. In particular, we demonstrate that the effect of a single phase-modulated pulse can be efficiently controlled by a suitably timed prepulse.

Due to the low laser intensity used in our experiment (5×10^9 W/cm^2), a weak field treatment of our experiment is sufficient. Because there are no intermediate resonant states, the interaction of our femtosecond laser pulses with the sodium atoms can be described by the simplified excitation scheme depicted in Fig. 1. The femtosecond laser pulse excites the 4*s* state from the 3*s* ground state by a two-photon transition. The 4*s* state population decays to the 3*p* state, which emits the sodium D-line (589 nm). The sodium D-line fluorescence serves as the observable. The control objective is the 4*s* population after the interaction with the femtosecond laser radiation and is assumed proportional to the sodium D-line fluorescence. We note that the observation of strong field effects using this excitation scheme might be obscured by averaging over spatial regions of different intensities. For example, in [32,33] it was demonstrated that the effect of spatial averaging can be circumvented by multiphoton detection schemes as only regions of higher intensities are sampled.

Our contribution is structured as follows. In Sec. I, the experimental setup is shown. In Sec. II, the theory is discussed. In Sec. III, our experimental results are presented. The contribution concludes with a summary in Sec. IV.

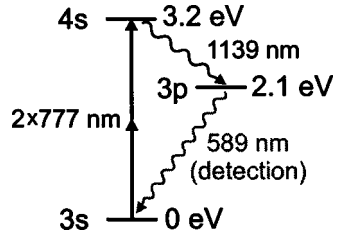

FIG. 1. Simplified excitation scheme of the sodium atoms. The two-photon excitation from the 3*s* ground state to the 4*s* state is two-photon resonant at 777 nm. Subsequent fluorescence from the 4*s* to the 3*p* and the 3*p* to the 3*s* states is depicted.

*Electronic address: baumert@physik.uni-kassel.de

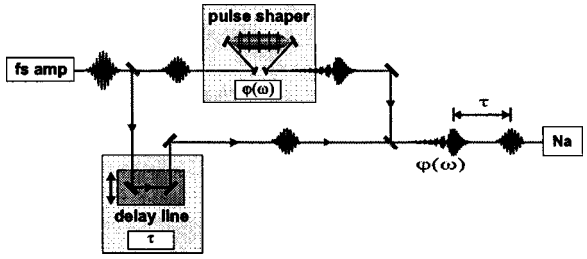

FIG. 2. Schematic experimental setup. The ultrashort laser pulses from a titanium-sapphire amplifier (fs amp) are sent into a Mach-Zehnder-interferometer with a delay line in one arm and a pulse shaper with a *CRI Inc*. 128-pixel liquid crystal spatial light modulator in the other arm. The recombined beam is directed into the sodium vapor cell (Na).

I. EXPERIMENTAL SETUP

A scheme of our experimental setup is shown in Fig. 2. The ultrashort laser pulses of about 30 fs full width at half maximum duration at 788 nm, 1 kHz repetition rate, and 1 mJ maximum energy per pulse were provided by a multipass titanium-sapphire amplifier. The incoming laser beam was directed into a Mach-Zehnder interferometer in order to generate a pair of pulses. The length of one arm was adjustable using a computer-controlled high-resolution delay line, whereas the beam in the other arm passed through our pulse shaper [34]. Thus, the delay τ between both arms and the spectral phase $\varphi(\omega)$ of the pulse passing through the pulse shaper were adjustable. Interferometric stability conditions were assured. After recombination, the unfocused laser beam with roughly 5 μJ pulse energy and 2 mm diameter (corresponding to 5×10^9 W/cm^2) was sent into a home-made low-pressure cell containing sodium vapor and argon at 5×10^{-2} mbar as a buffer gas. The working temperature was 350 °C, provided by direct electrical heating. The fluorescence radiation was collected through a window in a direction perpendicular to the laser beam propagation and detected by a photomultiplier tube. Using interference filters, only the sodium D-line emission was selected. After boxcar integration, the fluorescence signal was recorded as a function of the delay and the parameters of the spectral phase modulation. Besides the fluorescence signal, the intensity as well as the spectral amplitudes and phases were monitored using a power meter, spectral interference [35], and frequency-resolved optical gating [36].

II. THEORETICAL DESCRIPTION

The femtosecond laser pulses are described by their real temporal electric fields,

$$E(t) = \mathcal{E}(t)\ \cos[\omega_0\ t + \chi(t)], \tag{1}$$

consisting of the temporal pulse envelope $\mathcal{E}(t)$ and the temporal optical phase with the central laser frequency ω_0 and the relative temporal optical phase $\chi(t)$. The relative optical phase in a two-pulse experiment is illustrated in Fig. 3. The delay τ between the pulses determines the temporal separation between the envelopes of the pulses. The influence of

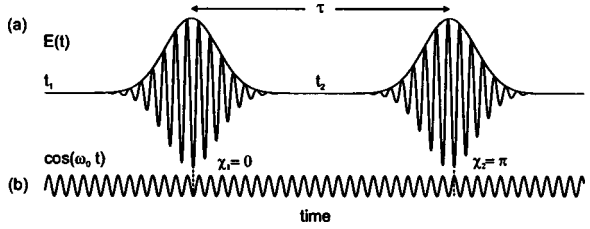

FIG. 3. Illustration of the relative temporal optical phase in a two-pulse experiment with (a) the real temporal electric field $E(t)$ and its envelope and (b) the carrier oscillation. The two pulses are separated in time by τ. χ_1 and χ_2 denote the constant relative temporal optical phases of the pulses.

the relative temporal optical phase can be seen by comparison of the electric field of each of the pulses with the carrier oscillation shown in Fig. 3(b). It shifts the oscillations of the electric field relative to the envelope and the carrier.

The spectral electric field is given by the Fourier transform of the temporal electric field,

$$\tilde{E}(\omega) = \int_{-\infty}^{\infty} E(t)e^{-i\omega t}\, dt. \tag{2}$$

A spectral phase modulation of an initial electric field $\tilde{E}_{in}(\omega)$ results in the outgoing modulated electric field,

$$\tilde{E}_{out}(\omega) = \tilde{E}_{in}(\omega)\ \exp\ [i\ \varphi(\omega)] \tag{3}$$

with the spectral optical phase $\varphi(\omega)$ of the modulation. For convenience, spectral phase modulations are always given for positive frequencies only, although the complete spectral phase modulation has to fulfill $\varphi(-\omega)=-\varphi(\omega)$. The resulting temporal electric field $E_{out}(t)$ is given by the inverse Fourier transform of $\tilde{E}_{out}(\omega)$.

In our experiments, we applied different phase functions $\varphi(\omega)$ and analyzed their influence on the final 4*s* state population. The time-dependent 4*s* state amplitude is given by

$$c_{4s}(t) = |c_{4s}(t)|\exp[i\ \xi_{4s}(t)], \tag{4}$$

where $|c_{4s}(t)|^2$ is the time-dependent 4*s* state population and $\xi_{4s}(t)$ is the time-dependent 4*s* state quantum-mechanical phase. The final ($t\to\infty$) 4*s* state population is denoted $|c_{4s}^{\infty}|^2$ and the phase ξ_{4s}^{∞}. In the following, we use the interaction picture in order to eliminate the time dependence $\exp(-i\omega_{4s\leftarrow3s}t)$ of the amplitudes when the laser is turned off. Here, $\omega_{4s\leftarrow3s}\approx4.85$ rad/fs is the transition frequency between the 3*s* and the 4*s* state.

We applied two different theoretical methods to describe the interaction of the femtosecond laser radiation with the sodium atoms in our experiments. The more general one is to solve the time-dependent Schrödinger equation numerically, while the more specific is second-order time-dependent perturbation theory, which is restricted to the weak-field regime. The direct numerical solution of the time-dependent Schrödinger equation was performed to assure the validity of perturbation theory. In both cases, the sodium D-line fluorescence is assumed proportional to the final population of the 4*s* state after the interaction with the femtosecond laser. The

final 4*s* population is investigated as a function of the control parameters, i.e., the delay and certain parameters of the spectral phase. In the weak-field regime, both methods agree and reproduce the experimental data.

To solve the time-dependent Schrödinger equation numerically, we employed the short-time-propagator method adapted for atoms from [37]. This means that the temporal amplitudes $c(t+\Delta t)$ of the sodium atom's states at a time $t+\Delta t$ are calculated by applying the short-time propagator $\exp[-(i/\hbar)\ H(t)\ \Delta t]$ with the step size Δt [typically 0.1 fs, in which $H(t)$ is assumed constant] to the temporal amplitudes $c(t)$ at the time t,

$$c(t+\Delta t) = \exp\left[-\frac{i}{\hbar}H(t)\ \Delta t\right]c(t). \tag{5}$$

The propagation amounts to the application of an exponential operator to the state vector. The Hamiltonian $H(t)$ consists of the unperturbed atomic Hamiltonian H_0 and the time-dependent interaction with the radiation field $V(t)$. The latter is described using the dipole approximation $V(t)=-\mu E(t)$, where μ describes the dipole moment operator and $E(t)$ is the real temporal electric field. In the next section, we use the short-time-propagator method to simulate the time-dependent population of the 4*s* state $|c_{4s}(t)|^2$ during the laser field interaction. In our simulations, all states from the ground state up to the principal quantum number 7 have been included using level data and transition probabilities from the *NIST Atomic Spectra Database*.

Within the weak-field regime, the two-photon transition from an initial state $|i\rangle$ to a final state $|f\rangle$ can be described by second order time-dependent perturbation theory [38]. If the intermediate states are sufficiently far from resonance, the final amplitude c_f^∞ can be approximated by [6,24,25]

$$c_f^\infty \propto \mathcal{S}[E^2(t)](\omega_{fi}) = \int_{-\infty}^{\infty} E^2(t)\exp[i\ \omega_{fi}\ t]dt \tag{6}$$

with the transition frequency ω_{fi}—in our case $\omega_{fi}=\omega_{4s\leftarrow 3s}$. This means that the final population $|c_{4s}^\infty|^2$ is proportional to the spectral components of the second harmonic at the transition frequency $|\mathcal{S}[E^2(t)](\omega_{fi})|^2$.

For the interpretation of spectral modulations, Eq. (6) can be rewritten as [24]

$$|c_f^\infty|^2 \propto \left|\int_{-\infty}^{\infty} \tilde{\mathcal{E}}\left(\frac{\omega_{fi}}{2}+\Omega\right)\tilde{\mathcal{E}}\left(\frac{\omega_{fi}}{2}-\Omega\right) \times \exp\left[i\left\{\varphi\left(\frac{\omega_{fi}}{2}+\Omega\right)+\varphi\left(\frac{\omega_{fi}}{2}-\Omega\right)\right\}\right]d\Omega\right|^2, \tag{7}$$

where the spectral electric field is $\tilde{E}(\omega)=\tilde{\mathcal{E}}(\omega)\exp[i\ \varphi(\omega)]$ with the spectral amplitude $\tilde{\mathcal{E}}(\omega)$ and the spectral phase $\varphi(\omega)$. It is shown in [25] that, as a consequence of Eq. (7), for all spectral phase functions $\varphi(\omega)$ which are antisymmetric around $\omega_{fi}/2$, the overall phase vanishes, leading to maximum population. In the next section, second-order time-dependent perturbation theory and the numerical solution of the time-dependent Schrödinger equation are used to interpret the experimental results.

III. EXPERIMENTAL RESULTS

In the first set of experiments, the delay of the interferometric pulse pair is varied while no spectral phase modulation is applied (see Sec. III A). Alternatively, a time delay between two pulses can also be realized applying a linear spectral phase (linear group delay modulation) [39]. Therefore, in the second set of experiments, the interferometric delay is set to zero and the Na D-line fluorescence is investigated as a function of the group delay (see Sec. III B). The differences between temporal delay and spectral group delay modulation are presented and analyzed. On the basis of this analysis, we show how the effect of a delay line is implemented with phase-modulation techniques. The results obtained in the time delay versus the group delay experiments indicate the importance of the relative temporal optical phase between the two pulses. To bring out this effect with greatest clarity, absolute spectral phase-modulation scans are performed at different interferometric delays in the third set of experiments (see Sec. III C). Delay, group delay modulation, and absolute phase modulation form the basis for the understanding of more complex spectral phase modulations. In the last set of experiments, we study periodic sinusoidal and discontinuous π-jump spectral phase modulations with two pulses and discuss the observations in light of the previous results (see Secs. III D and III E).

A. Interferometric delay

Without spectral phase modulation, the combined electric field is the sum of two identical pulses $E(t)+E(t-\tau)$ separated by the delay τ which is set by the delay line. Inserting this into Eq. (6) results in

$$|c_f^\infty(\tau)|^2 \propto |\mathcal{S}_{qm}(\tau)+\mathcal{S}_{opt}(\tau)|^2 \tag{8}$$

with

$$\mathcal{S}_{qm}(\tau) = (1+\exp[i\ \omega_{fi}\ \tau])\mathcal{S}[E^2(t)](\omega_{fi}) \tag{9}$$

and

$$\mathcal{S}_{opt}(\tau) = 2\ \mathcal{S}[E(t)E(t-\tau)](\omega_{fi}) = 2\int_{-\infty}^{\infty} E(t)E(t-\tau)\exp[i\ \omega_{fi}\ t]dt, \tag{10}$$

where $\mathcal{S}_{qm}(\tau)$ and $\mathcal{S}_{opt}(\tau)$ denote the quantum-mechanical and the optical contribution. The optical contribution vanishes if the pulses do not overlap in time.

For different ranges of the delay, different types of interferences are observed in the experiment. In Fig. 4(a), delays around $\tau=0$ are presented. Here, optical interferences with a period of 2.6 fs corresponding to half of the transition frequency are observed. Since both the pulses overlap in time, they interfere optically, i.e., the shape of the electric fields varies with τ. The separate analysis of the optical and the quantum-mechanical contribution gives further insights (Fig.

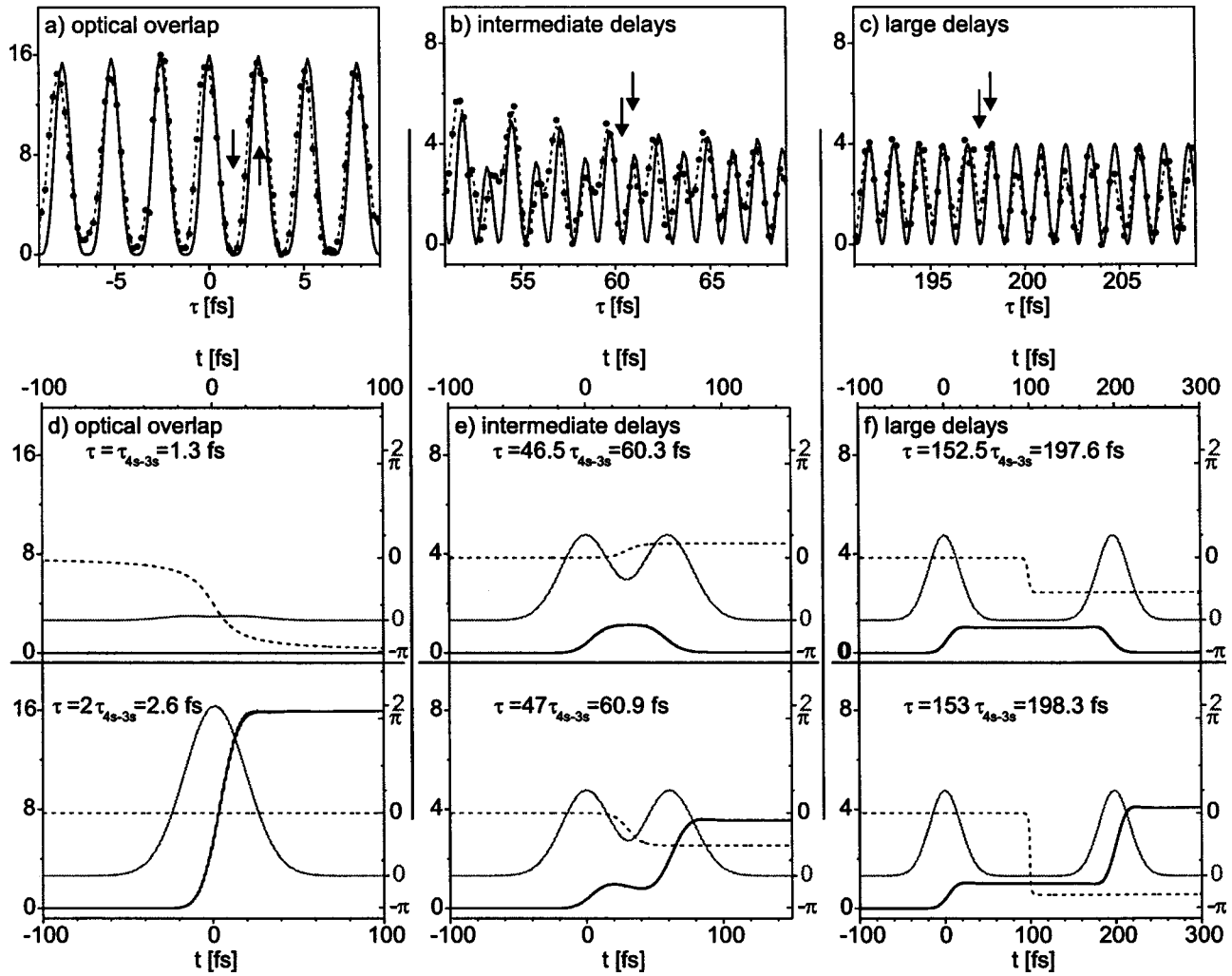

FIG. 4. Interferometric delay: The upper row shows the sodium D-line fluorescence signal ($\propto$4*s* population) as a function of the delay: close to the optical overlap (a), for intermediate (b), and large delays (c). The signal is normalized so that a single bandwidth limited pulse generates a unity signal. Solid lines are calculated using Eq. (6) while the dashed lines with the dots present measured data. In the lower row, time-dependent 4*s* populations calculated with Eq. (5) for different delays are shown. The chosen delays are indicated by the arrows in (a)–(c). For each range of the delay [(d)–(f)], examples of destructive (upper part) and constructive interference (lower part) have been calculated. Besides the 4*s* populations (solid black lines with values at the left side of each graph), the corresponding temporal pulse envelopes $\mathcal{E}(t)$ (solid gray lines with gray values at the right side of each graph, outgoing ticks) and their relative temporal phases $\chi(t)$ (dashed lines with values at the right side of each graph, ingoing ticks) are depicted. For the electric fields, Gaussian pulses of 30 fs full width at half maximum duration at a central wavelength of 788 nm are used.

5). The optical contribution has a slowly varying absolute value vanishing for large delays and is oscillating with half the transition frequency [see Figs. 5(a) and 5(b)]. The absolute value of the quantum-mechanical contribution oscillates with the transition frequency. Its phase is linear with a slope equal to the transition frequency [see Fig. 5(c)]. In the case of a population maximum, $\mathcal{S}_{qm}(\tau)$ and $\mathcal{S}_{opt}(\tau)$ sum up constructively. As an example, the delay of 2.6 fs is marked in Figs. 5(b) and 5(c) by small black circles. Here, both the optical and the quantum-mechanical contribution have zero phase. At the population minima seen in Fig. 4(a), $\mathcal{S}_{qm}(\tau)$ and $\mathcal{S}_{opt}(\tau)$ interfere destructively. Here, the optical and the quantum-mechanical contribution have a phase difference of π. This can be seen, for example, at the delay of 1.3 fs, which is also indicated by small black circles in Figs. 5(b) and 5(c).

With increasing delay, the overlap of both pulses decreases and, thus, $\mathcal{S}_{opt}(\tau)$ decays to zero [Fig. 5(a)] and the additional maxima of $\mathcal{S}_{qm}(\tau)$ appear in the combined signal. This is why the quantum interferences [6] of $\mathcal{S}_{qm}(\tau)$ with a period of $\tau_{4s-3s} \approx 1.3$ fs corresponding to the transition frequency are more pronounced for increasing delays [see additional maxima in Fig. 4(b)]. At large delays, when both pulses are completely separated in time, there are no optical interferences, i.e., the optical part $\mathcal{S}_{opt}(\tau)$ is zero. Only quantum interferences are observed. The population is therefore given by $|\mathcal{S}_{qm}(\tau)|^2$ [see Fig. 4(c)].

To elucidate the physical mechanism, the time-dependent population of the 4s state is investigated using the short-time-propagator method [see Eq. (5)]. In Figs. 4(d)–4(f), the time-dependent 4*s* population and corresponding temporal pulse envelopes and their relative optical phases are plotted

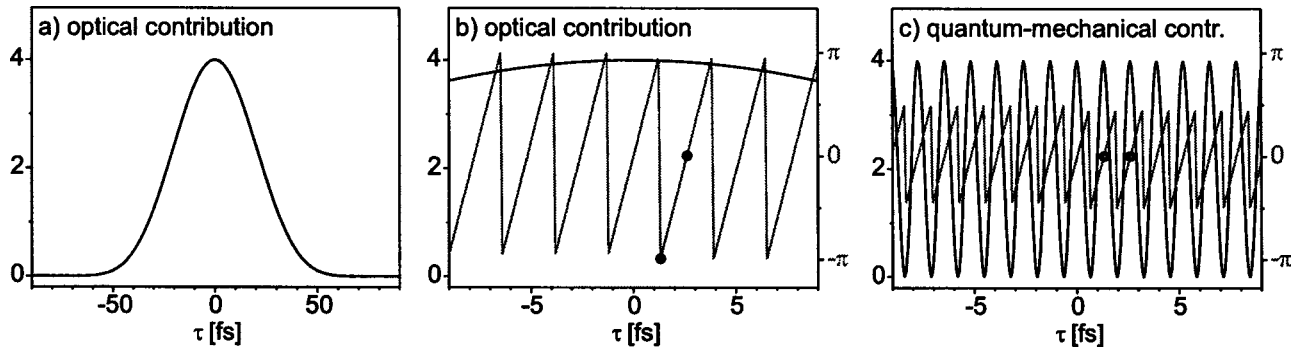

FIG. 5. Interferometric delay: optical contribution $\mathcal{S}_{opt}(\tau)$ and quantum-mechanical contribution $\mathcal{S}_{qm}(\tau)$ for a Gaussian pulse (30 fs full width at half maximum temporal duration at a central wavelength of 788 nm). In (a), $|\mathcal{S}_{opt}(\tau)|^2$ is depicted. In addition to the square of the absolute value, the wrapped phases (gray lines with values at the right side of the graphs) are shown for the optical (b) and the quantum-mechanical contribution (c), respectively. The small black circles indicate delays where the optical contribution and the quantum-mechanical contribution interfere destructively (1.3 fs) and constructively (2.6 fs), respectively.

for different delays. Figure 4(d) refers to the optical regime with small delays. Both pulses interfere optically due to their temporal overlap so that the final 4*s* state oscillates between maximum and zero at a period of 1.3 fs. Quantum interferences give rise to different population dynamics depicted in Figs. 4(e) and 4(f). Since both pulses still overlap at a delay around 50 fs, the combined action of optical and quantum interferences is observed. The upper part of Fig. 4(e) shows that the 4*s* state is populated by the first pulse and depopulated by the second pulse at $\tau=60.3$ fs. The lower part at a delay of 60.9 fs corresponds to constructive quantum interference. Purely quantum interferences at large delays are shown in Fig. 4(f). The first pulse populates the 4*s* state without optically interfering with the second pulse. Depending on its relative optical phase, the second pulse further populates or depopulates the 4*s* state. Note that the optical phases are not $-\pi/2$ and $-\pi$ in Fig. 4(f) since the laser frequency and the transition are nonresonant.

B. Group delay modulation

In contrast to Sec. III A, here we use a linear spectral phase to shift the laser pulse in time. We consider a linear group delay modulation

$$\varphi(\omega) = T_{GD}(\omega - \omega_{ref}) \tag{11}$$

with the group delay GD and the reference frequency ω_{ref}. As known from femtosecond optics [40,41], a group delay modulation shifts the envelope of the temporal electric field by the group delay for all reference frequencies,

$$E_{\mathrm{GD}}(t) = \mathcal{E}(t + T_{\mathrm{GD}})\cos[\omega_0\, t + T_{\mathrm{GD}} \cdot (\omega_0 - \omega_{ref})]. \tag{12}$$

The experimental results show that the final 4*s* population cannot be controlled by shifting the pulse envelope. In Fig. 6(a), the group delay is scanned with the reference frequency taken at half the transition frequency, i.e., $\omega_{ref} \approx \omega_{4s\leftarrow 3s}/2 \approx 2.42$ rad/fs (corresponding to 777 nm). Almost no modulation of the 4*s* state population is observed, although the pulse envelope is shifted in time in a range of 100 fs similarly to the interferometric delay, scan. In the case of $\omega_{ref} = \omega_{4s\leftarrow 3s}/2$, the quantum-mechanical interferences are always constructive. In the frequency domain, this result is interpreted in terms of the antisymmetry of $\varphi(\omega)$ around $\omega_{4s\leftarrow 3s}/2$. Thus, the quantum-mechanical phase difference is not changed by the group delay. In the next experiment, ω_{ref} was set to 2.35 rad/fs (corresponding to 800 nm). Here, slow modulations with a period of $2\pi/|2\omega_{ref} - \omega_{4s\leftarrow 3s}| \approx 45$ fs are observed since the spectral phase around $\omega_{4s\leftarrow 3s}/2$ and, therefore, the quantum-mechanical phase change slightly [see Fig. 6(c)]. The difference between the interferometric delay and the group delay spectral modulation becomes clearly apparent in the time-dependent pictures. In Fig. 4(e), the two pulses have been separated by the delay line while they have been separated by the spectral group delay modulation in Figs. 6(b) and 6(d). In both cases, the temporal separations between both pulses have been chosen equal to 60.3 fs and 60.9 fs, respectively. In the case of the interferometric delay, the relative temporal phases of the electric field vary significantly from 60.3 fs to 60.9 fs and, thus, the final 4*s* populations. However, for the group delay modulations, these phases vary only slightly, resulting in nearly constant final 4*s* populations. This means that the relative temporal phase between the pulses controls the final 4*s* population. These results highlight the differences between delays produced by a delay line and delays generated with spectral phase-modulation techniques. In particular, we find that by choosing $\omega_{ref}=0$, a delay line can be emulated by the pulse shaper, resulting in the same types of interferences [cf. Figs. 6(e)–6(g) with Figs. 4(a)–4(c) and Eq. (12)].

C. Absolute phase modulation

To further elucidate the role of the relative temporal phase, we performed absolute spectral phase scans at different delays. In the absolute spectral phase-modulation experiments, the spectral phase is constant for all frequencies,

$$\varphi(\omega) = \varphi_0, \tag{13}$$

and φ_0 is the control parameter. In the time domain, the absolute spectral phase modulation corresponds to a shift of the relative temporal optical phase by φ_0 while the pulse remains at the position given by the delay,

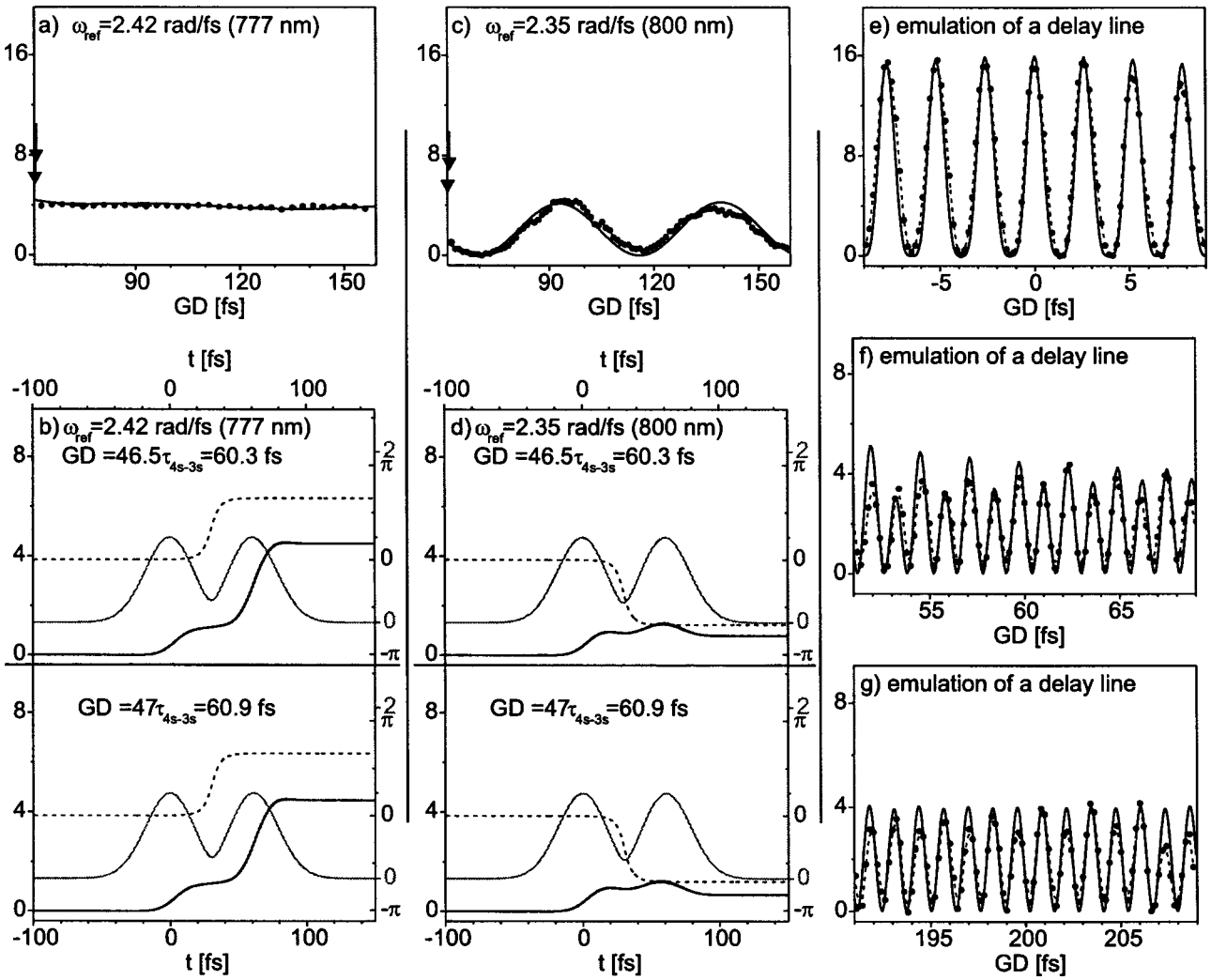

FIG. 6. Spectral group delay modulations: Group delay scans and time-dependent 4*s* populations for $\omega_{ref}=2.42$ rad/fs and 2.35 rad/fs are presented in (a)–(d). The arrows in (a) and (c) indicate the group delays used in the time-dependent 4*s* populations shown in (b) and (d): $N_{\mathrm{GD}}=60.3$ fs and 60.9 fs. (e)–(g) show different ranges of the group delay for $\omega_{ref}=0$ so that a delay line is emulated.

$$E_{abs}(t)=\mathcal{E}(t-\tau)\cos[\omega_0\,(t-\tau)+\varphi_0]. \tag{14}$$

This means that exclusively the relative temporal phase difference between both pulses is varied by scanning φ_0 (cf. Fig. 3). In Figs. 7(a), 7(b), and 7(d), scans of the absolute phase at different positions of the delay line—small, intermediate, and large delay—are presented. In the case of the small delay when both pulses overlap in time, optical interferences are observed, while for intermediate and large delays the quantum interferences with the quantum-mechanical phase difference of $\Delta\xi_{4s}^{\infty}=2\varphi_0$ become the dominant type of interference. This means that the temporal separation between both pulses determines the type of interferences while the temporal phase difference between both pulses is the control parameter for the final 4*s* population. The influence of the temporal phase can be further seen in the time-dependent populations in Fig. 7(c). Depending on φ_0, the second pulse depopulates or further populates the 4*s* state. The combination of a delay line with linear and absolute spectral phase modulations provides the physical background to analyze more complex phase-modulation functions, as discussed in the following.

D. Sinusoidal modulation

Sinusoidal spectral phase modulations of a single pulse have proven to be effective in controlling multiphoton processes [24]. Applications to larger molecules and two-photon microscopy have been reported as well [18,31]. Moreover, sinusoidal modulations were combined with an evolutionary algorithm to control a different two-photon transition in sodium [26]. Sinusoidal spectral modulation is given by

$$\varphi(\omega)=A\,\sin[T(\omega-\omega_{ref})+\phi] \tag{15}$$

with the amplitude A, the time constant T, and the phase ϕ of the sine function. This spectral modulation results in a pulse sequence in the time domain. Using the identity

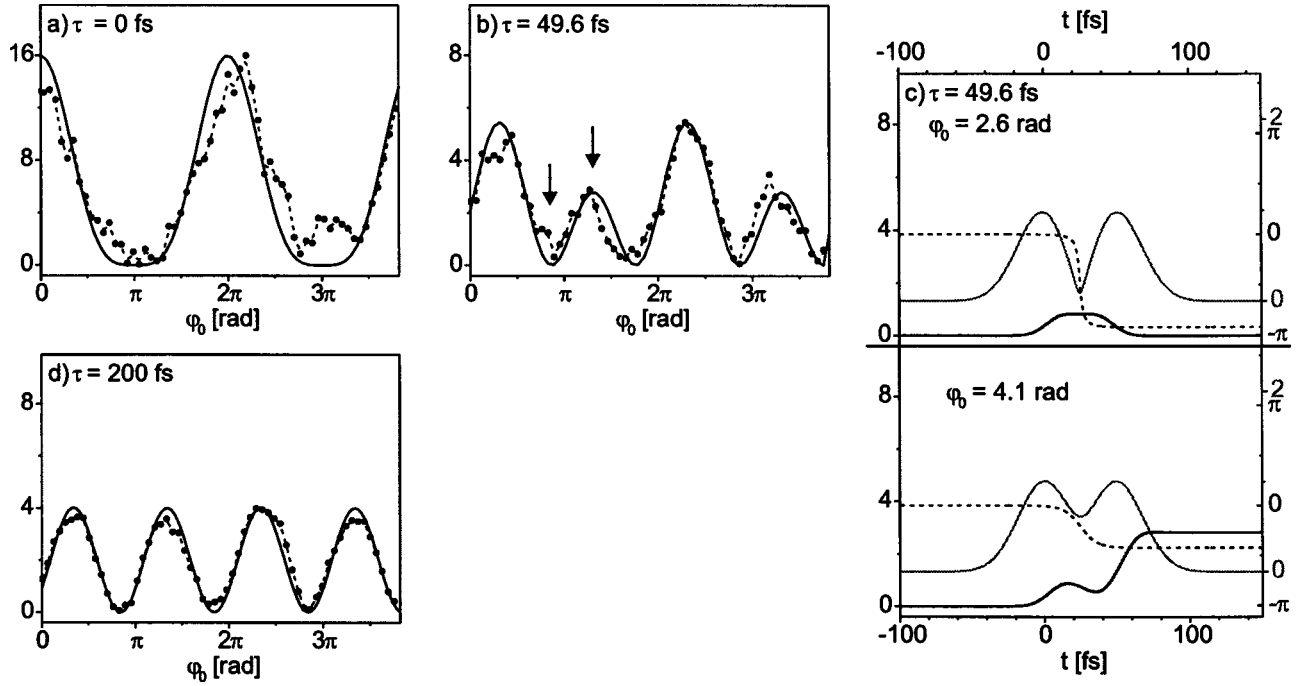

FIG. 7. Absolute spectral phase modulations: Scans of the absolute spectral phase φ_0 at the delays $\tau=0$ fs, 49.6 fs, and 200 fs between the two pulses are shown in (a), (b), and (d). The arrows in (b) indicate the absolute phases used in the time-dependent 4*s* populations presented in (c). Besides the 4*s* populations (solid black lines with values at the left side of each graph), the corresponding temporal pulse envelopes $\mathcal{E}(t)$ (solid gray lines with gray values at the right side of each graph, outgoing ticks) and their relative temporal phases $\chi(t)$ (dashed lines with values at the right side of each graph, ingoing ticks) are depicted in (c).

$$\exp\{i\,A\,\sin[T(\omega-\omega_{ref})+\phi]\} = \sum_{n=-\infty}^{\infty} J_n(A)\exp\{in[T(\omega-\omega_{ref})+\phi]\}, \qquad (16)$$

where $J_n(A)$ is the Bessel function of the first kind and order n, the modulated temporal electric field is given by

$$E_{\sin}(t) = \sum_{n=-\infty}^{\infty} J_n(A)\;\mathcal{E}(t+nT)\cos\{\omega_0\,t+n\,[T\,(\omega_0-\omega_{ref}) + \phi]\}. \qquad (17)$$

Therefore, T is equal to the temporal separation between the pre- and post-pulses and the amplitude A determines how much energy is transferred from the central pulse to the pre- and post-pulses. Changing the phase of the sine function ϕ alters the temporal relative optical phases of the subpulses and, thus, determines whether the amplitude of the 4*s* state interferes constructively or destructively during the pulse sequence. First, we obtain similar results to Ref. [24] for only one phase-modulated pulse, i.e., the other arm of the interferometer is blocked. In Figs. 8(a) and 8(b), scans of ϕ for $\varphi(\omega)=A\,\sin[200\;fs\;(\omega-\omega_{4s\leftarrow 3s}/2)+\phi]$ with $A=0.8$ and $A=\pi$ are presented. The temporal separation $T=200$ fs was chosen so that the subpulses do not overlap in time. Therefore, no optical interferences between the subpulses are present. For both sine amplitudes, the population has a maximum for $\phi=0$ because $\varphi(\omega)$ is antisymmetric around $\omega_{4s\leftarrow 3s}/2$. In Fig. 8(c), time-dependent populations of the 4*s* state are presented for a sine amplitude $A=\pi$. Depending on their relative temporal phases, the subpulses populate and depopulate the 4*s* state as seen in the previous section for the case of two pulses and absolute spectral phase modulation. In Fig. 8(a) ($A=0.8$), there is no completely destructive interference because the energy of the central pulse is too high and therefore the population created during the central pulse cannot be eliminated by destructive interference due to the pre- and postpulses.

After the systematic study of the influence of the parameter of the sinusoidal spectral phase modulation with one pulse, the more complex two-pulse experiment with one pulse sinusoidally modulated and the other pulse shifted in time by the delay line is investigated. The delay line is set to about 300 fs so that the pulse from the delay line comes before the sinusoidally modulated pulse and does not temporally overlap with a subpulse from the pulse sequence generated by the sinusoidal modulation. In Figs. 8(d) and 8(e), the experimental results of the Na D-line fluorescence as a function of ϕ at two slightly different delays are presented. The results shown in Fig. 8(d) with $\tau=300.6$ fs are very similar to the single-pulse experiment [cf. Fig. 8(a)], whereas the signal modulation in Fig. 8(e) with $\tau=300.1$ fs is significantly reduced. The change of the modulation for different temporal delays is explained by further analysis of the quantum-mechanical interferences using Eqs. (6) and (8), respectively. If the unshaped pulse $E_1(t)$ and the shaped pulse $E_2(t)$ do not overlap in time, the optical interference term vanishes so that the final 4*s* population is given by

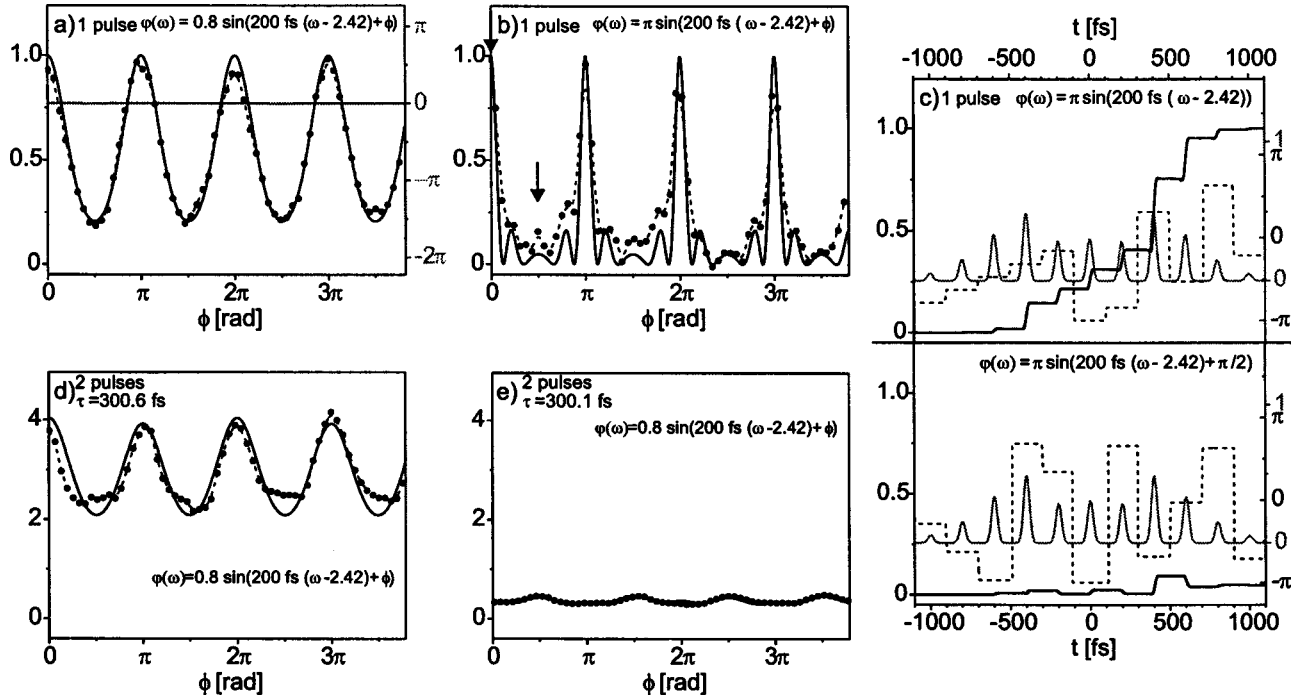

FIG. 8. Sinusoidal spectral phase modulations: (a) and (b) show scans of ϕ for a single pulse. Besides the 4*s* population (solid black line), the final quantum-mechanical phase $\xi_{4s,2}^{\infty}$ (solid gray line), i.e., after the interaction with the single modulated pulse, as a function of ϕ is presented in (a) with gray values at the right side of the graph. In (c), two time-dependent 4*s* populations and the corresponding temporal pulse envelopes and phases have been calculated for different ϕ (single pulse). (d) and (e) are scans of ϕ with two pulses at different delays: 300.6 fs and 300.1 fs.

$$
\begin{aligned}
|c_{4s}^{\infty}|^2 &\propto |\mathcal{S}[E_1^2(t)](\omega_{fi}) + \mathcal{S}[E_2^2(t)](\omega_{fi})|^2 \\
&= |\mathcal{S}[E_1^2(t)](\omega_{fi})|^2 + |\mathcal{S}[E_2^2(t)](\omega_{fi})|^2 \\
&\quad + 2|\mathcal{S}[E_1^2(t)](\omega_{fi})|\,|\mathcal{S}[E_2^2(t)](\omega_{fi})|\cos(\Delta\xi_{4s}^{\infty}).
\end{aligned}
\tag{18}
$$

In Eq. (18) , $|\mathcal{S}[E_1^2(t)]|^2$ is constant, $|\mathcal{S}[E_2^2(t)]|^2$ depends on the spectral phase modulation, while $2|\mathcal{S}[E_1^2(t)]|\,|\mathcal{S}[E_2^2(t)]|\cos(\Delta\xi_{4s}^{\infty})$ describes the quantum-mechanical interaction of both pulses by the quantum-mechanical phase difference $\Delta\xi_{4s}^{\infty}=\xi_{4s,2}^{\infty}-\xi_{4s,1}^{\infty}$ where $\xi_{4s,1}^{\infty}$ and $\xi_{4s,2}^{\infty}$ are the quantum-mechanical phases resulting from the nonmodulated and the modulated pulse, respectively. In Fig. 8(a), the quantum-mechanical phase $\xi_{4s,2}^{\infty}$ resulting from the modulated pulse is plotted in addition to the population. For the used sinusoidal modulation, it does not depend on ϕ. Therefore, the quantum-mechanical phase difference $\Delta\xi_{4s}^{\infty}$ depends solely on the delay and is equal to $\omega_{4s\leftarrow 3s}\,\tau$ for all ϕ. As a consequence, depending on the delay, the shaped pulse interferes quantum mechanically constructively or destructively with the delay line arm pulse for all ϕ—resulting in strong or weak modulation. This means that a suitable timed initial pulse strongly influences the degree of controllability that can be achieved with the phase-modulated pulse. Here, the sinusoidal phase modulation served as a first example.

The analysis of the results obtained in the experiment on an unmodulated pulse and a delayed sinusoidally spectral phase-modulated pulse is generally applicable for other types of spectral phase modulations as well. In the next section, we investigate the combined action of an unmodulated pulse and a π-jump spectral phase-modulated pulse as a second example.

E. π-jump modulation

π-jump modulation means that the spectral phase is set to zero for all frequencies smaller than a reference frequency ω_{π} and to π for all frequencies larger than ω_{π}. In a two-photon transition experiment, such a modulation can generate dark pulses, i.e., pulses which result in the final population being equal to zero [25]. First, we investigate the effect of a single π-jump modulated pulse similar to the experiments of [25]. Then, we expand to the corresponding two-pulse experiment. Here, we demonstrate how the effect of single-pulse control can be inverted by another suitably timed pulse.

The temporal electric field of a π-jump modulated pulse has a "double half-pulse structure" depending on ω_{π} [see Fig. 9(b)]. The results of the single-pulse experiment where ω_{π} is scanned are plotted in Fig. 9(a). For $\omega_{\pi}=\omega_{4s\leftarrow 3s}/2$, the population is maximum since the spectral phase modulation is antisymmetric. At each side of $\omega_{4s\leftarrow 3s}/2$, a dark pulse can be observed. The corresponding time-dependent populations are shown in Fig. 9(b). The first half-pulse populates the 4*s* state while the second half-pulse populates or depopulates the 4*s* state.

The results of the two-pulse experiment are shown in Figs. 9(c) and 9(d). In Fig. 9(c), ω_{π} is varied while the delay

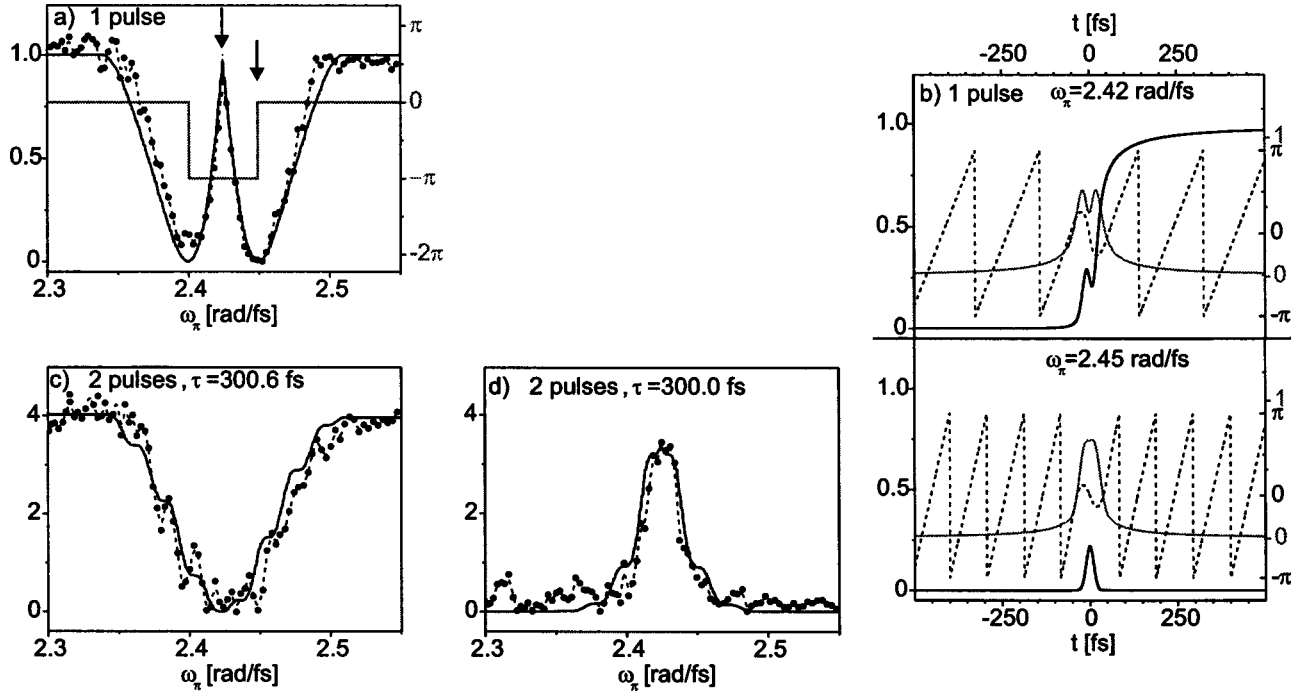

FIG. 9. Spectral π-jump modulations. In (a), the 4*s* population and the final quantum-mechanical phase $\xi^{\infty}_{4s,2}$ for a single pulse π-jump scan is presented. (b) shows the time-dependent 4*s* populations, the temporal pulse envelopes, and optical phases for two different ω_{π} indicated by the arrows in (a). Phase wrapping of the optical phase is employed for display. (c) and (d) are two-pulse π-jump scans for different delays.

between both pulses is set to 300.6. The result is a central hole for $\omega_{\pi}=\omega_{4s\leftarrow 3s}/2$. Slightly changing the delay to 300.0 completely inverts the control. As a consequence, the observed hole in Fig. 9(c) is converted into a hill as seen in Fig. 9(d).

As before, this effect is explained by analyzing the final quantum-mechanical phase $\xi^{\infty}_{4s,2}$ after the interaction with the single modulated pulse. In the single-pulse experiment, the quantum-mechanical phase at the inner part between the dark pulses differs by π from the phase at the outer part [see the phase in Fig. 9(a)]. In the case of Fig. 9(c), the additional pre-pulse is 300.6 fs before the shaped pulse. At this delay, the final quantum-mechanical phase resulting from the interaction with only the nonshaped prepulse is $\xi^{\infty}_{4s,1}=0$, while $\xi^{\infty}_{4s,2}$ from the shaped pulse has the structure shown in Fig. 9(a). Thus, the quantum-mechanical phase difference $\Delta\xi^{\infty}_{4s}$ is $-\pi$ for the inner part around $\omega_{\pi}=\omega_{4s\leftarrow 3s}/2$ and zero for the outer part, i.e., there is destructive interference for the inner part and constructive interference for the outer part. Therefore, the resulting 4*s* state population in the two-pulse experiments is a hole as shown in Fig. 9(c).

In Fig. 9(d), the delay is 300.0 fs so that $\xi^{\infty}_{4s,1}$ is $-\pi$. In this case, destructive interference occurs at the outer part ($\Delta\xi^{\infty}_{4s}=\pi$) while there is constructive interference for the inner part ($\Delta\xi^{\infty}_{4s}=0$), i.e., destructive and constructive interference between the inner and the outer part are exchanged and the hole is converted into a hill. This demonstrates that despite the complex structure of the two-pulse π-jump modulation scan, the results can be explained by reduction to the single-pulse experiment and the delay line scan in combination with the quantum-mechanical phase difference.

IV. SUMMARY

Phase control of a two-photon transition with shaped femtosecond laser pulse sequences was studied in detail on the two-photon transition $4s\leftarrow\leftarrow 3s$ on sodium atoms. The final 4*s* state population was the control objective while the sodium D-line fluorescence was the observable. Besides the final 4*s* populations as functions of the control parameters, the dynamics of the 4*s* population during the laser interaction were discussed for all experiments. First, regarding the relative temporal optical phases and the 4*s* population dynamics, the analogies and differences between an interferometric delay generated by a delay line and the linear spectral group delay phase modulation by a pulse shaper were presented. Thereby, we demonstrate how the physical effect of a delay line is properly emulated by the pulse shaper. Additional investigation of the absolute spectral phase modulation demonstrated the role of the relative temporal optical phase. The relative temporal phase was the fundamental control parameter of the excited state's population while the temporal separation between the pulse envelopes determined the type of interferences. The dynamics induced by a pulse sequence generated by a sinusoidal spectral phase modulation were reduced to this interpretation. The corresponding two-pulse experiment with an additional delayed pulse showed that the additional pulse can significantly influence the controllability. Depending on its delay, the additional pulse determines the amount of control exerted by the shaped pulse. This effect highlighted the role of the quantum-mechanical phase. One pulse defines the reference quantum-mechanical phase while the other pulse excites with a relative phase. This leads to constructive and destructive quantum-mechanical interfer-

ences, especially seen in the time-dependent 4*s* populations.

Besides the sinusoidal modulation, the discontinuous π-jump modulation was extended to a two-pulse experiment. Here, an additional pulse was capable of inverting the control effect by a single shaped pulse. Again, the control effects were discussed in terms of the quantum-mechanical phase.

We demonstrated that by decomposing complex excitation scenarios into more elementary steps, the basic physical mechanisms are revealed. One of the fascinating aspects of the combination of phase-locked pulses with phase-modulation techniques is the ability to "control the control" with a precisely timed prepulse.

ACKNOWLEDGMENTS

The technical assistance of D. Liese, the support of the Deutsche Forschungsgemeinschaft, and the NRC-Helmholtz program are gratefully acknowledged.

[1] A. H. Zewail, J. Phys. Chem. A **104**, 5660 (2000).
[2] S. A. Rice and M. Zhao, *Optimal Control of Molecular Dynamics* (Wiley-Interscience, New York, 2000).
[3] M. Shapiro and P. Brumer, *Principles of the Quantum Control of Molecular Processes* (Wiley, Hoboken, NJ, 2003).
[4] H. Rabitz, R. de Vivie-Riedle, M. Motzkus, and K. Kompa, Science **288**, 824 (2000).
[5] M. Wollenhaupt, A. Assion, D. Liese, Ch. Sarpe-Tudoran, T. Baumert, S. Zamith, M. A. Bouchene, B. Girard, A. Flettner, U. Weichmann, and G. Gerber, Phys. Rev. Lett. **89**, 173001 (2002).
[6] V. Blanchet, C. Nicole, M.-A. Bouchene, and B. Girard, Phys. Rev. Lett. **78**, 2716 (1997).
[7] P. Tian, D. Keusters, Y. Suzaki, and W. S. Warren, Science **300**, 1553 (2003).
[8] K. Ohmori, Y. Sato, E. E. Nikitin, and S. A. Rice, Phys. Rev. Lett. **91**, 243003 (2003).
[9] N. F. Scherer, R. J. Carlson, A. Matro, M. Du, A. J. Ruggiero, V. Romero-Rochin, J. A. Cina, G. R. Fleming, and S. A. Rice, J. Chem. Phys. **95**, 1487 (1991).
[10] R. Netz, A. Nazarkin, and R. Sauerbrey, Phys. Rev. Lett. **90**, 063001 (2003).
[11] S. Mukamel, *Principles of Nonlinear Optical Spectroscopy* (Oxford University Press, New York, 1995).
[12] C. Fang, J. Wang, Y. S. Kim, A. K. Charnley, W. Barber-Armstrong, A. B. Smith III, S. M. Decatur, and R. M. Hochstrasser, J. Phys. Chem. B **108**, 10 415 (2004).
[13] A. M. Weiner, Prog. Quantum Electron. **19**, 161 (1995).
[14] A. M. Weiner, Rev. Sci. Instrum. **71**, 1929 (2000).
[15] M. A. Dugan, J. X. Tull, and W. S. Warren, in *Advances in Magnetic and Optical Resonance*, edited by W. S. Warren (Academic Press, San Diego, 1997), Vol. 20, pp. 1–65.
[16] R. S. Judson and H. Rabitz, Phys. Rev. Lett. **68**, 1500 (1992).
[17] A. Assion, T. Baumert, M. Bergt, T. Brixner, B. Kiefer, V. Seyfried, M. Strehle, and G. Gerber, Science **282**, 919 (1998).
[18] J. L. Herek, W. Wohlleben, R. J. Cogdell, D. Zeidler, and M. Motzkus, Nature (London) **417**, 533 (2002).
[19] T. C. Weinacht, J. Ahn, and P. H. Bucksbaum, Phys. Rev. Lett. **80**, 5508 (1998).
[20] C. Daniel, J. Full, L. González, C. Lupulescu, J. Manz, A. Merli, Š. Vajda, and L. Wöste, Science **299**, 536 (2003).
[21] R. J. Levis, G. M. Menkir, and H. Rabitz, Science **292**, 709 (2001).
[22] C. J. Bardeen, V. V. Yakovlev, K. R. Wilson, S. D. Carpenter, P. M. Weber, and W. S. Warren, Chem. Phys. Lett. **280**, 151 (1997).
[23] T. Brixner, T. Pfeifer, G. Gerber, M. Wollenhaupt, and T. Baumert, *Femtosecond Laser Spectroscopy*, Kluwer Series on Progress in Lasers (Kluwer, Dordrecht, 2004), pp. 229–271.
[24] D. Meshulach and Y. Silberberg, Nature (London) **396**, 239 (1998).
[25] D. Meshulach and Y. Silberberg, Phys. Rev. A **60**, 1287 (1999).
[26] T. Hornung, R. Meier, D. Zeidler, K.-L. Kompa, D. Proch, and M. Motzkus, Appl. Phys. B: Lasers Opt. **71**, 277 (2000).
[27] N. Dudovich, B. Dayan, S. M. Gallagher Faeder, and Y. Silberberg, Phys. Rev. Lett. **86**, 47 (2001).
[28] T. Brixner and G. Gerber, Opt. Lett. **26**, 557 (2001).
[29] N. Dudovich, D. Oron, and Y. Silberberg, Phys. Rev. Lett. **92**, 103003 (2004).
[30] T. Brixner, G. Krampert, T. Pfeifer, R. Selle, G. Gerber, M. Wollenhaupt, O. Graefe, C. Horn, D. Liese, and T. Baumert, Phys. Rev. Lett. **92**, 208301 (2004).
[31] I. Pastirk, J. M. Dela Cruz, K. A. Walowicz, V. V. Lozovoy, and M. Dantus, Opt. Express **11**, 1695 (2003).
[32] T. Frohnmeyer, M. Hofmann, M. Strehle, and T. Baumert, Chem. Phys. Lett. **312**, 447 (1999).
[33] M. Wollenhaupt, A. Assion, O. Bazhan, Ch. Horn, D. Liese, Ch. Sarpe-Tudoran, M. Winter, and T. Baumert, Phys. Rev. A **68**, 015401 (2003).
[34] A. Präkelt, M. Wollenhaupt, A. Assion, Ch. Horn, C. Sarpe-Tudoran, M. Winter, and T. Baumert, Rev. Sci. Instrum. **74**, 4950 (2003).
[35] L. Lepetit, G. Chériaux, and M. Joffre, J. Opt. Soc. Am. B **12**, 2467 (1995).
[36] R. Trebino, *Frequency-Resolved Optical Gating: The Measurement of Ultrashort Laser Pulses* (Kluwer Academic Publishers, Norwell, 2000).
[37] B. M. Garraway and K.-A. Suominen, Rep. Prog. Phys. **58**, 365 (1995).
[38] R. Loudon, *The Quantum Theory of Light*, 2nd ed. (Clarendon Press, Oxford, 1990).
[39] A. W. Albrecht, J. D. Hybl, S. M. Gallagher Faeder, and D. M. Jonas, J. Chem. Phys. **111**, 10 934 (1999).
[40] J. C. Diels and W. Rudolph, *Ultrashort Laser Pulse Phenomena* (Academic Press, San Diego, 1996).
[41] M. Wollenhaupt, A. Assion, and T. Baumert, *Femtosecond Laser Pulses: Linear Properties, Manipulation, Generation and Measurement*, Springer Handbook of Lasers and Optics (Springer, Berlin, in press).